Article

Theoretical Studies on the Magnetic Switching Controlled by Stacking Patterns of Bis(maleonitriledithiolato) Nickelate(III) Dimers

Zhaoping Ni, Xiaoming Ren, Jing Ma, Jingli Xie, Chunlin Ni, Zhida Chen, and Qingjin Meng

J. Am. Chem. Soc., **2005**, 127 (41), 14330-14338• DOI: 10.1021/ja050631z • Publication Date (Web): 23 September 2005

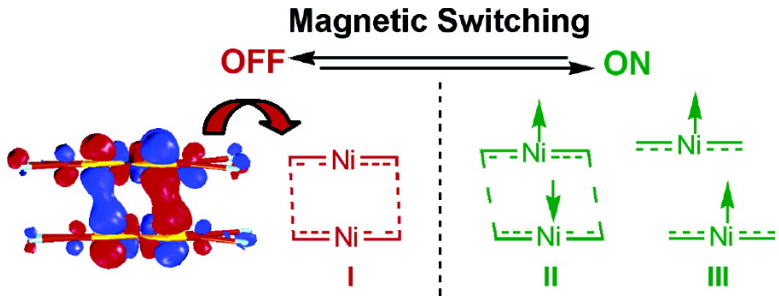

More About This Article

Additional resources and features associated with this article are available within the HTML version:

- Supporting Information
- Links to the 3 articles that cite this article, as of the time of this article download
- Access to high resolution figures
- Links to articles and content related to this article
- Copyright permission to reproduce figures and/or text from this article

View the Full Text HTML

J|A|C|S
ARTICLES
Published on Web 09/23/2005

Theoretical Studies on the Magnetic Switching Controlled by Stacking Patterns of Bis(maleonitriledithiolato) Nickelate(III) Dimers

Zhaoping Ni,[†] Xiaoming Ren,[†] Jing Ma,*[,‡] Jingli Xie,[†] Chunlin Ni,[†] Zhida Chen,[§] and Qingjin Meng*[,†]

Contribution from the Coordination Chemistry Institute, State Key Laboratory of Coordination Chemistry, and Institute of Theoretical and Computational Chemistry, Key Laboratory of Mesoscopic Chemistry of MOE, Nanjing University, Nanjing, 210093, P. R. China, and State Key Laboratory of Rare Earth Materials Chemistry and Applications, College of Chemistry and Molecular Engineering, Peking University, Beijing, 100871, P. R. China

Received January 31, 2005; E-mail: majing@nju.edu.cn; mengqj@nju.edu.cn

Abstract: Magnetic switchable maleonitriledithiolate (mnt) complexes were studied by density functional theory. The calculations were performed for anion dimers of [RBzPyR′][Ni(mnt)$_2$] (RBzPyR′ = derivatives of benzylpyridinium) to elucidate magnetostructural correlations and the nature of the weak intermolecular chemical bonding. The calculated results showed that the spin delocalization, favored by the eclipsed stacking and the shorter interlayer distance, was responsible for the diamagnetic character of [1-benzyl-4-aminopyridinium][Ni(mnt)$_2$] at low temperature. The weak antiferromagnetic and ferromagnetic interactions were also reproduced for [1-benzyl-4-aminopyridinium][Ni(mnt)$_2$] and [1-(4′-fluorobenzyl)pyridinium][Ni(mnt)$_2$] at high temperature, respectively. The natural bond orbital analysis suggested that the cooperative effect of the weak intermolecular bondings may be the intrinsic driving force resulting in the switchable property, which is essentially similar to those in organic radicals exhibiting magnetic bistability. Further investigations with varying interlayer distance *d*, the extent of slippage (slipping distance *r* and deviation angle α), and rotational angle θ suggested that the extent of slippage played an important role in magnetic interactions. Therefore, the abrupt modulation of the extent of slippage in the [Ni(mnt)$_2$]$^-$ complexes by external perturbations provided new possibilities for the design of molecular magnetic switching devices.

Introduction

The discovery of molecular switches is mostly stimulated by their potential applications in molecular electronics.[1] Especially, rapid and reversible changes with bistable character in optical, electrical, or magnetic switches are frequently used for memory or sensing applications.[2] Spin-crossover compounds, a kind of well-known molecular bistability materials, have attracted considerable interest with a high potential for such purpose.[3] Moreover, their spin-crossover temperature can be adjusted to around ambient temperature by choosing suitable counteranions and ligands.[4] Although the origin of the bistability is molecular, the shape of spin transition curve is dependent on intermolecular interactions.[5] The discovery of the room-temperature magnetic bistability in an organic radical, 1,3,5-trithia-2,4,6-triazapentalenyl, owing to intermolecular dimerization, opened a new branch in this field.[6] In particular, the alkyl-substituted spirobiphenalenyl radicals display that optical, electrical, and magnetic properties can be simultaneously switched.[7] However, the nature

[†] Coordination Chemistry Institute and State Key Laboratory, Nanjing University.

[‡] Institute of Theoretical and Computational Chemistry, Nanjing University.

[§] Peking University.

(1) (a) Pease, A. R.; Jeppesen, J. O.; Stoddart, J. F.; Luo, Y.; Collier, C. P.; Heath, J. R. *Acc. Chem. Res.* **2001**, *34*, 433. (b) Carroll, R. L.; Gorman, C. B. *Angew. Chem., Int. Ed.* **2002**, *41*, 4378. (c) Bousseksou, A.; Molnár, G.; Matouzenko, G. *Eur. J. Inorg. Chem.* **2004**, 4353. (d) de Silva, A. P.; McClenaghan, N. D. *Chem.—Eur. J.* **2004**, *10*, 574. (e) Roubeau, O.; Colin, A.; Schmitt, V.; Clérac, R. *Angew. Chem., Int. Ed.* **2004**, *43*, 3283.

(2) (a) de Silva, A. P.; Gunaratne, H. Q. N.; Gunnlaugsson, T.; Huxley, A. J. M.; McCoy, C. P.; Rademacher, J. T.; Rice, T. E. *Chem. Rev.* **1997**, *97*, 1515. (b) Coe, B. J. *Chem.—Eur. J.* **1999**, *5*, 2464. (c) Photochromism: Memories and Switches Special Issue. *Chem. Rev.* **2000**, *100*, 1683. (d) Malaun, M.; Reeves, Z. R.; Paul, R. L.; Jeffery, J. C.; McCleverty, J. A.; Ward, M. D.; Asselberghs, I.; Clays, K.; Persoons, A. *Chem. Commun.* **2001**, 49. (e) Sato, O. *Acc. Chem. Res.* **2003**, *36*, 692. (f) Niel, V.; Thompson, A. L.; Muñoz, M. C.; Galet, A.; Goeta, A. E.; Real, J. A. *Angew. Chem., Int. Ed.* **2003**, *42*, 3760. (g) Sporer, C. et al. *Angew. Chem., Int. Ed.* **2004**, *43*, 5266. (h) Dei, A.; Gatteschi, D.; Sangregorio, C.; Sorace, L. *Acc. Chem. Res.* **2004**, *37*, 827. (i) Sato, O.; Kawakami, T.; Kimura, M.; Hishiya, S.; Kubo, S.; Einaga, Y. *J. Am. Chem. Soc.* **2004**, *126*, 13176.

(3) (a) Gütlich, P.; Hauser, A.; Spiering, H. *Angew. Chem., Int. Ed. Engl.* **1994**, *33*, 2024. (b) Renz, F.; Oshio, H.; Ksenofontov, V.; Waldeck, M.; Spiering, H.; Gütlich, P. *Angew. Chem., Int. Ed.* **2000**, *39*, 3699. (c) Gütlich, P.; Garcia, Y.; Woike, T. *Coord. Chem. Rev.* **2001**, *219−221*, 839. (d) Garcia, Y.; Moscovici, J.; Michalowicz, A.; Ksenofontov, V.; Levchenko, G.; Bravic, G.; Chasseau, D.; Gütlich, P. *Chem.—Eur. J.* **2002**, *8*, 4992. (e) Glaser, T. *Angew. Chem., Int. Ed.* **2003**, *42*, 5668.

(4) (a) Kröber, J.; Codjovi, E.; Kahn, O.; Grolière, F.; Jay, C. *J. Am. Chem. Soc.* **1993**, *115*, 9810. (b) Kahn, O.; Martinez, C. J. *Science* **1998**, *279*, 44.

(5) (a) Hauser, A.; Jeftić, J.; Romstedt, H.; Hinek, R.; Spiering, H. *Coord. Chem. Rev.* **1999**, *190−192*, 471. (b)Spiering, H.; Kohlhaas, T.; Romstedt, H.; Hauser, A.; Bruns-Yilmaz, C.; Kusz, J.; Gütlich, P. *Coord. Chem. Rev.* **1999**, *190−192*, 629. (c) Real, J. A.; Gaspar, A. B.; Niel, V.; Muñoz, M. C. *Coord. Chem. Rev.* **2003**, *236*, 121.

(6) (a) Fujita, W.; Awaga, K. *Science* **1999**, *286*, 261. (b) Fujita, W.; Awaga, K.; Matsuzaki, H.; Okamoto, H. *Phys. Rev. B* **2002**, *65*, 064434. (c) Brusso, J. L.; Clements, O. P.; Haddon, R, C.; Itkis, M. E.; Leitch, A. A.; Oakley, R. T.; Reed, R. W.; Richardson, J. F. *J. Am. Chem. Soc.* **2004**, *126*, 8256.

 10.1021/ja050631z CCC: $30.25

Scheme 1

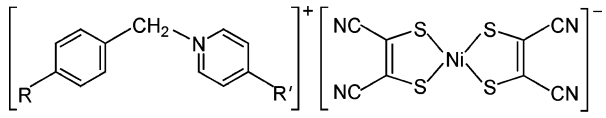

1

of the intermolecular interactions that generate the necessary cooperativity in this kind of radical materials is not well understood.[8] The planar metal-bis-1,2-dithiolene complexes, configurationally similar to some organic materials,[6c] have been widely investigated in the areas of conducting and magnetic materials, dyes, nonlinear optics, and catalysis.[9] Promising features enable them to be building blocks of new multiproperty switches. Complexes of the maleonitriledithiolate (mnt) ligand, one of the most widely studied families of dithiolene complexes, have the ability to stack into flexible one-dimensional chains in the solid state.[9a−c,10] Recently, several unusual abrupt paramagnetic-diamagnetic phase transitions have been observed in the $[RBzPyR']^+[Ni(mnt)_2]^-$ (RBzPyR′ = derivatives of benzylpyridinium) complexes **1** as shown in Scheme 1.[11] They are phenomenologically similar to the transition behaviors observed in some spin-crossover materials[5c,12] but essentially similar to those in the radical materials.[6,8] Furthermore, changing the substituent groups in the RBzPyR′ cation resulted in different patterns of stacking column of $[Ni(mnt)_2]^-$ anions. Consequently, various magnetic behaviors such as spin Peierls-like transition, metamagnetic-like behavior, and ferromagnetic ordering were obtained.[13] To explore the magnetostructural correlations, Manoharan used the extended Hückel method for the $[Ni(mnt)_2]^-$ dimer in such content.[14] The observation of ferromagnetic ordering in $NH_4[Ni(mnt)_2]\cdot H_2O$ below 4.5 K was associated with the pressure dependence of the Curie temperature. The understanding of this phenomenon using UHF/INDO and RHF/INDO/SD-CI quantum calculations[15] has renewed both experimental and theoretical interest in dithiolene based compounds.[10,16] Density functional theory (DFT) studies for exploring the electronic structures of metal dithiolene complexes in their ground states have been reported.[17] Further explorations of the relationship among packing patterns, magnetic behaviors, and the nature of weak chemical intermolecular bonding are interesting and challenging issues for chemists.[18]

Herein we chose three different packing patterns of $[Ni(mnt)_2]^-$ anions: **2** with 1-benzyl-4-aminopyridinium cation[11a] (R = H, R′ = NH_2) at low temperature (**2-LT**) and high temperature (**2-HT**) experimental structures, respectively, and **3** with 1-(4′-fluorobenzyl) pyridinium cation[11b] (R = F, R′ = H) at high temperature (**3-HT**) as illustrated in Figure 1. (The detailed X-ray structures are shown in Table S1.) The magnetic behaviors of **2-LT** and **2-HT** represent two states after and before switching, respectively,[11a] which are phenomenologically similar to some six-coordinate Fe(II) spin-crossover complexes.[5c,12] Despite the unsuccessful measurement of the crystal structural data in the low temperature for complex **3**, the first-order crystallographic phase transition was confirmed by the variable-temperature X-ray diffraction experiments,[11b] which is associated with the peculiar magnetic transition from ferromagnetic coupling to diamagnetism. Therefore, they are potential magnetic switching devices whereby the "off" states would correspond to zero magnetic susceptibilities and the "on" states to nonzero values.[3−6,12] In this work, we attempt to understand the origin of the magnetic switching for $[Ni(mnt)_2]^-$ complexes and how the stacking patterns affect magnetic transitions. Density functional theory combined with the broken-symmetry approach[19] was used to explore the effects of several factors such as the interlayer distance *d*, extent of slippage (slipping distance *r* and deviation angle α), and rotational angle *θ* as defined in Figure 1a on magnetic behaviors. The nature of transition between a paramagnetic high-temperature phase and a diamagnetic low-temperature phase is probed by magnetic interactions, spin density distributions, natural orbital (NO) analysis,[19b,20] and natural bond orbital (NBO) analysis.[21] The packing patterns based on several model structures are also investigated.

(7) (a) Chi, X.; Itkis, M. E.; Kirschbaum, K.; Pinkerton, A. A.; Oakley, R. T.; Cordes, A. W.; Haddon, R. C. *J. Am. Chem. Soc.* **2001**, *123*, 4041. (b) Itkis, M. E.; Chi, X.; Cordes, A. W.; Haddon, R. C. *Science* **2002**, *296*, 1443. (c) Miller, J. S. *Angew. Chem., Int. Ed.* **2003**, *42*, 27.

(8) Brusso, J. L.; Clements, O. P.; Haddon, R, C.; Itkis, M. E.; Leitch, A. A.; Oakley, R. T.; Reed, R. W.; Richardson, J. F. *J. Am. Chem. Soc.* **2004**, *126*, 14692.

(9) (a) Robertson, N.; Cronin, L. *Coord. Chem. Rev.* **2002**, *227*, 93. (b) Kato, R. *Chem. Rev*. **2004**, *104*, 5319. (c) Fourmigué, M. *Acc. Chem. Res.* **2004**, *37*, 179. (d) Wang, K.; Stiefel, E. I. *Science* **2001**, *291*, 106. (e) Fan, Y. B.; Hall, M. B. *J. Am. Chem. Soc.* **2002**, *124*, 12076. (f) Akutagawa, T. et al. *J. Am. Chem. Soc.* **2005**, *127*, 4397.

(10) (a) Rovira, C. et al. *Angew. Chem., Int. Ed. Engl.* **1997**, *36*, 2324. (b) Pullen, A. E.; Faulmann, C.; Pokhodnya, K. I.; Cassoux, P.; Tokumoto, M.; *Inorg. Chem.* **1998**, *37*, 6714. (c) Ribera, E. et al. *Chem. Eur. J*. **1999**, *5*, 2025. (d) Ribas, X. et al. *Adv. Funct. Mater*. **2005**, *15*, 1023.

(11) (a) Ren, X. M.; Meng, Q. J.; Song, Y.; Hu, C. J.; Lu, C. S.; Chen, X. Y.; Xue, Z. L. *Inorg. Chem*. **2002**, *41*, 5931. (b) Xie, J. L.; Ren, X. M.; Song, Y.; Zhang, W. W.; Liu, W. L.; He, C.; Meng, Q. J. *Chem. Commun.* **2002**, 2346. (c) Ni, C. L.; Dang, D. B.; Li, Y. Z.; Yuan, Z. R.; Ni, Z. P.; Tian, Z. F.; Meng, Q. J. *Inorg. Chem. Commun.* **2004**, *7*, 1034.

(12) (a) Holland, J. M.; McAllister, J. A.; Lu, Z. B.; Kilner, C. A.; Thornton-pett, M.; Halcrow, M. A. *Chem. Commun.* **2001**, 577. (b) Zhu, D. R.; Xu, Y.; Yu, Z.; Guo, Z. J.; Sang, H.; Liu, T.; You, X. Z. *Chem. Mater*. **2002**, *14*, 838.

(13) (a) Ren, X. M.; Meng, Q. J.; Song, Y.; Lu, C. S.; Hu, C. J.; Chen, X. Y. *Inorg. Chem.* **2002**, *41*, 5686. (b) Xie, J. L.; Ren, X. M.; He, C.; Song, Y.; Meng, Q. J.; Kremer, R. K.; Yao, Y. G. *Chem. Phys. Lett*. **2003**, *369*, 41. (c) Xie, J. L.; Ren, X. M.; Gao, S.; Zhang, W. W.; Li, Y. Z.; Lu, C. S.; Ni, C. L.; Liu, W. L.; Meng, Q. J.; Yao, Y. G. *Eur. J. Inorg. Chem*. **2003**, 2393. (d) Xie, J. L.; Ren, X. M.; Song, Y.; Zou, Y.; Meng, Q. J. *J. Chem. Soc., Dalton Trans*. **2002**, 2868.

(14) Lalitha, S.; Bhavani, R.; Chandramouli, G. V. R.; Manoharan, P. T. *THEOCHEM* **1996**, *361*, 161.

(15) Coomber, A. T.; Beljonne, D.; Friend, R. H.; Brédas, J. L.; Charlton, A.; Robertson, N.; Underhill, A. E.; Kurmoo, M.; Day, P. *Nature* **1996**, *380*, 144.

(16) (a) Hayes, R. G. *Inorg. Chem*. **2000**, *39*, 156. (b) Stein, M.; van Lenthe, E.; Baerends, E. J.; Lubitz, W. *J. Phys. Chem. A* **2001**, *105*, 416. (c) Devic, T.; Domercq, B.; Auban-Senzier, P.; Molinié, P.; Fourmigué, M. *Eur. J. Inorg. Chem*. **2002**, 2844. (d) Stadler, C.; de Lacey, A. L.; Hernández, B.; Fernández, V. M.; Conesa, J. C. *Inorg. Chem*. **2002**, *41*, 4417. (e) Waters, T.; Wang, X. B.; Yang, X.; Zhang, L. Y.; O'Hair, R. A. J.; Wang, L. S.; Wedd, A. G. *J. Am. Chem. Soc.* **2004**, *126*, 5119. (f) Nakajima, H.; Katsuhara, M.; Ashizawa, M.; Kawamoto, T.; Mori, T. *Inorg. Chem*. **2004**, *43*, 6075. (g) Staniland, S. S.; Fujita, W.; Umezono, Y.; Awaga, K.; Camp, P. J.; Clark, S. J.; Robertson, N. *Inorg. Chem*. **2005**, *44*, 546.

(17) (a) Lim, B. S.; Fomitchev, D. V.; Holm, R. H. *Inorg. Chem*. **2001**, *40*, 4257. (b) Szilagyi, R. K.; Lim, B. S.; Glaser, T.; Holm, R. H.; Hedman, B.; Hodgson, K. O.; Solomon, E. I. *J. Am. Chem. Soc.* **2003**, *125*, 9158. (c) Ray, K.; Begum, A.; Weyhermüller, T.; Piligkos, S.; van Slageren, J.; Neese, F.; Wieghardt, K. *J. Am. Chem. Soc.* **2005**, *127*, 4403.

(18) (a) Huang, J. S.; Kertesz, M. *J. Am. Chem. Soc.* **2003**, *125*, 13334. (b) Brocks, G. *J. Chem. Phys.* **2000**, *112*, 5353. (c) Novoa, J. J.; Lafuente, P.; Del Sesto, R. E.; Miller, J. S. *Angew. Chem., Int. Ed.* **2001**, *40*, 2540. (d) Del Sesto, R. E.; Miller, J. S.; Lafuente, P.; Novoa, J. J. *Chem.—Eur. J.* **2002**, *8*, 4894. (e) Takano, Y.; Taniguchi, T.; Isobe, H.; Kubo, T.; Morita, Y.; Yamamoto, K.; Nakasuji, K.; Takui, T.; Yamaguchi, K. *J. Am. Chem. Soc.* **2002**, *124*, 11122.

(19) (a) Noodleman, L.; Norman, J. G., Jr. *J. Chem. Phys*. **1979**, *70*, 4903. (b) Nagao, H.; Nishino, M.; Shigeta, Y.; Soda, T.; Kitagawa, Y.; Onishi, T.; Yoshioka, Y.; Yamaguchi, K. *Coord. Chem. Rev.* **2000**, *198*, 265. (c) Ciofini, I.; Dual, C. A. *Coord. Chem. Rev.* **2003**, *238−239*, 187.

(20) (a) Soda, T.; Kitagawa, Y.; Onishi, T.; Takano, Y.; Shigeta, Y.; Nagao, H.; Yoshioka, Y.; Yamaguchi, K. *Chem. Phys. Lett*. **2000**, *319*, 223. (b) Takano, Y.; Kitagawa, Y.; Onishi, T.; Yoshioka, Y.; Yamaguchi, K.; Koga, N.; Iwamura, H. *J. Am. Chem. Soc*. **2002**, *124*, 450.

(21) (a) Reed, A. E.; Curtiss, L. A.; Weinhold, F. *Chem. Rev.* **1988**, *88*, 899. (b) Montejo, M.; Navarro, A.; Kearley, G. J.; Vázquez, J.; López-González, J. J. *J. Am. Chem. Soc.* **2004**, *126*, 15087.

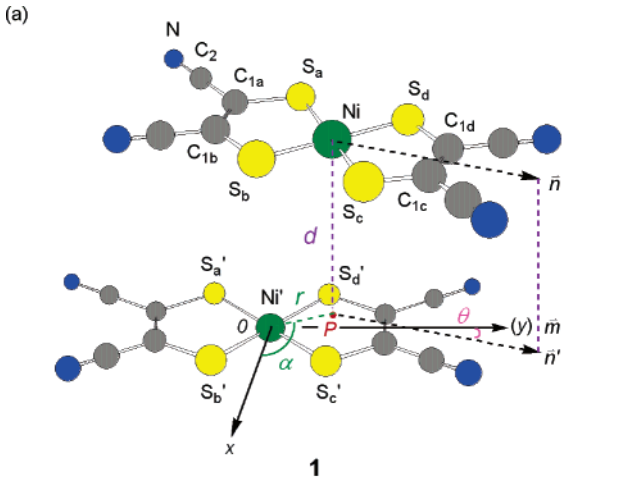

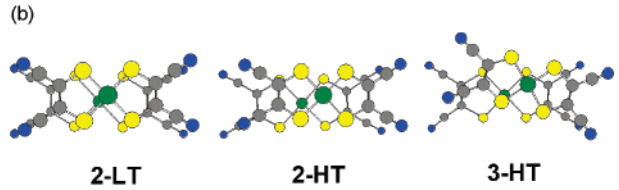

dimer	d (Å)	r (Å)	α (°)	θ (°)
2-LT	3.48	0.72	128	2
2-HT	3.65	1.44	110	3
3-HT	3.55	1.75	114	13

Figure 1. (a) Packing parameters for $[Ni(mnt)_2]^-$ dimer of **1** (counterions are omitted for clarity). $\vec{n}$ and $\vec{m}$ are the axes of symmetry of planar $[Ni(mnt)_2]^-$ monomer passing through metal atoms in the upper and lower layers, respectively. *P* point and $\vec{n}'$ axis are the vertical projection of the upper Ni atom and axis to the lower layer, respectively. The structure of $[Ni(mnt)_2]^-$ dimer can be parametrized by interlayer distance *d*, the extent of slippage (slipping distance *r* and deviation angle α) and rotational angle θ. (b) The X-ray crystal structures of $[Ni(mnt)_2]^-$ dimers **2-LT**, **2-HT** (complex **2** with 1-benzyl-4-aminopyridinium cation at 89 K and 293 K, respectively[11a]), and **3-HT** (complex **3** with 1-(4′-fluorobenzyl)pyridinium cation at 298 K[11b]).

Theoretical Background

Magnetic Coupling Constant. The interaction between two magnetic centers can be described with the Heisenberg−Dirac−van Vleck Hamiltonian model:[22]

$$\hat{H} = -2J_{ab}\vec{S}_a\vec{S}_b \tag{1}$$

where J_{ab} is the magnetic coupling between the unpaired electrons in sites a and b. The broken-symmetry DFT strategy has been applied as a practical tool for the study of magnetic interactions on rather large systems with reasonable accuracy and partial considerations of the electron correlation effects.[19] Assuming the so-called "weak bonding" regime, Noodleman et al.[23] evaluate the magnetic coupling within broken symmetry framework by

$$J_{ab}^{(1)} = \frac{E_{BS} - E_T}{S_{max}^{\ 2}} \tag{2}$$

where E_{BS} and E_T denote the total energies in the broken-symmetry (BS) singlet state and triplet state, respectively, and S_{max} corresponds to the total spin of the high-spin state. However, in the strong overlap region, it has been suggested that the following expression might give more reasonable solutions.[24]

$$J_{ab}^{(2)} = \frac{E_{BS} - E_T}{S_{max}(S_{max} + 1)} \tag{3}$$

The approximate spin projection procedure involving the expectation value of the total spin angular momentum $\langle S^2 \rangle$ has also been introduced to evalute J_{ab} values[19b,20]

$$J_{ab}^{(3)} = \frac{E_{BS} - E_T}{\langle S^2 \rangle_T - \langle S^2 \rangle_{BS}} \tag{4}$$

where $\langle S^2 \rangle_T$ and $\langle S^2 \rangle_{BS}$ denote the total spin angular momentum of triplet state and broken-symmetry singlet state, respectively. If the singlet and triplet states are equally mixed, $\langle S^2 \rangle_{BS}$ is equal to 1.0, while, in the closed-shell system, $\langle S^2 \rangle_{BS} = 0$. It should be noted that $\langle S^2 \rangle$ is a typical two-electron property, whereas the Kohn−Sham (KS) Slater determinant corresponds to a one-particle quantity for the noninteracting system. The correct evaluation of $\langle S^2 \rangle$ within the DFT framework is still an open question.[25] However, Wang et al. found that the $\langle S^2 \rangle$ values from the KS Slater determinant, though not exact, are reasonable for high-spin radicals.[26]

Molecular Orbital Pictures of Magnetic Switching. The interactions between the unpaired electrons in the $[Ni(mnt)_2]^-$ dimer are schematically depicted in Figure 2. The energy gap between the intermolecular bonding and antibonding dimer orbitals consisting of the singly occupied molecular orbitals (SOMO) of the $[Ni(mnt)_2]^-$ monomers is crucial to the magnetic interaction.[18c−e] If the effect of orbital overlap in the $[Ni(mnt)_2]^-$ dimer is dominant, the energy gap is large and both α and β spin electrons enter the bonding dimer orbital, resulting in a diamagnetic form **I** (DM). If the energy gap is small, electrons partially enter the antibonding dimer orbital, leading to the weak antiferromagnetic (AFM) interaction in **II**. As the orbital overlap is negligible, electrons enter the MOs in a parallel manner according to Hund's rule, affording the ferromagnetic (FM) interaction in **III**. So abrupt transitions from **II** to **I** or from **III** to **I** influenced by the external environment, such as temperature, pressure, or light irradiation, will lead to a magnetic switching property.[6−8,11]

Natural Orbital (NO) and Natural Bond Orbital (NBO) Analyses. For the estimate of the relative contribution between spin delocalization and polarization effects, natural orbital analysis was utilized.[19b,20] The NOs of DFT solutions are obtained by diagonalizing their first-order density matrices with n_i denoting the occupation number of *i*th NO. The magnetic orbitals $\psi_i^{\pm}$ are obtained by the linear combinations of the

(22) (a) Heisenberg, W. Z. *Phys.* **1928**, *49*, 619. (b) Dirac, P. A. M. *The principles of quantum mechanics*; Clarendon Press: Oxford, U.K., 1947. (c) Van Vleck, J. H. *The theory of electric and magnetic susceptibilities*; Oxford University Press: Oxford, U.K., 1932.
(23) (a) Ginsberg, A. P. *J. Am. Chem. Soc.* **1980**, *102*, 111. (b) Noodleman, L. *J. Chem. Phys.* **1981**, *74*, 5737. (c) Noodleman, L.; Davidson, E. R. *Chem. Phys.* **1986**, *109*, 131.
(24) (a) Bencini, A.; Totti, F.; Daul, C. A.; Doclo, K.; Fantucci, P.; Barone, V. *Inorg. Chem.* **1997**, *36*, 5022. (b) Ruiz, E.; Cano, J.; Alvarez, S.; Alemany, P. *J. Comput. Chem.* **1999**, *20*, 1391.
(25) (a) Gräfenstein, J.; Hjerpe, A. M.; Kraka, E.; Cremer, D. *J. Phys. Chem. A* **2000**, *104*, 1748. (b) Gräfenstein, J.; Cremer, D. *Mol. Phys.* **2001**, *99*, 981.

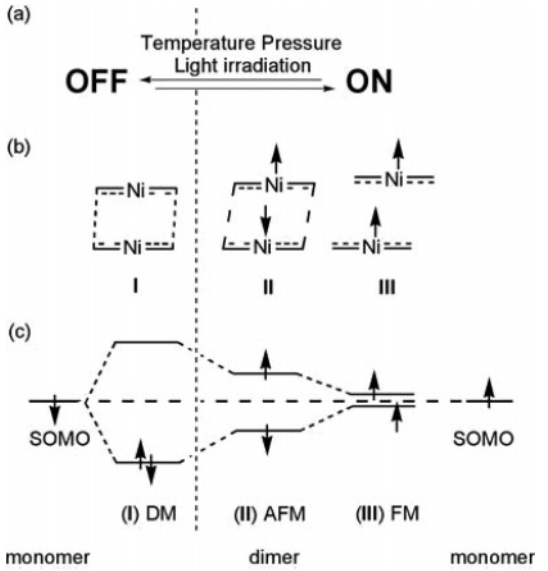

Figure 2. Schematic pictures of SOMO−SOMO interaction schemed for (**I**) diamagnetic (DM), (**II**) antiferromagnetic interaction (AFM), and (**III**) ferromagnetic interaction (FM); abrupt transition from **II** to **I** or from **III** to **I** will lead to the switchable property.

bonding and antibonding NO. The orbital overlap $T_i = \langle \psi_i^+ | \psi_i^- \rangle$ can approximately scale the spin delocalization. It can be obtained by the following relationship:

$$T_i = n_i - 1,\ T_i = 1 - n^*_i \qquad (5)$$

$T_i = 1$ stands for the upper limit of the extent of spin delocalization in dimers. The spin polarization effect comes from a secondary interaction, resulting in the partial transfer of electrons between HOMO and LUMO. Essentially, effects of spin delocalization and polarization are controlled by the overlap of SOMO orbitals and the energy difference between the HOMO and LUMO orbitals, respectively.

NBO analysis has been demonstrated as a useful tool to provide chemists with a quantitative description of intermolecular interactions in accordance with the classical Lewis structure concepts and with the basic Pauling−Slater−Coulson pictures of bond hybridization and polarization.[21] In the present work, we use NBO analysis to quantitatively describe the weak bonding interaction in the $[Ni(mnt)_2]^-$ dimer. The natural localized molecular orbitals/natural population analysis (NLMO/NPA) can directly illustrate the formation of the weak bond between two layers.

Computational Details

In this study, several DFT functionals such as the local spin density approach (SVWN), the generalized gradient approximations (BP86, BPW91, and BLYP), and the hybrid functional methods (B2LYP,[27] B3LYP, B3PW91) with the LANL2DZ basis set were employed. Judging by the J_{ab} values, we found that SVWN, BP86, and BPW91 provide reasonable results for **2-LT**, **2-HT**, and **3-HT** (cf. Tables S2−S4). To examine the basis set dependence of the DFT results, we performed BPW91 calculations with CEP-31G, LANL2DZ, and LANL2DZ for the complex with one set of f-polarization functions[28] adding to the Ni atom (ECP1), LANL2DZ for the Ni atom and the 6-31G* basis set for the remaining atoms (ECP2), SDD, and 6-311G with the results shown in Table S5. It can be found that all the basis sets give similar performance. Therefore, we employ BPW91/LANL2DZ results throughout the article to discuss the magnetic interactions and intermolecular interactions in $[Ni(mnt)_2]^-$ dimers. The convergence criterion of SCF is 10^{-8}. In some cases, SCF convergence difficulties could be alleviated by decreasing the convergence criterion of SCF to 10^{-7}. All computations are carried out with Gaussian 98[29] including the NBO program[30] on SGI 3800 and 3000 workstations. Because the initial guess is different between Gaussian 98 and Gaussian 03,[31] we also compare the results from the two programs for **2-LT**, **2-HT**, and **3-HT** in Table S2 and Table S4.[32] The Harris functional used as the initial guess[33] in Gaussian 03 program may be more suitable for weakly interacting system. The program MOLDEN 3.8[34] is used for visualization of orbitals.

Magnetic Interactions in the Switchable $[Ni(mnt)_2]^-$ Dimer

Strength of Magnetic Interactions. To measure the magnitude of the magnetic interactions, we estimate the J_{ab} values with three schemes for **2-LT**, **2-HT**, and **3-HT** as shown in Table S2. The results indicate that the $J_{ab}^{(1)}$ and $J_{ab}^{(3)}$ values are close in the strong localized limit, while the $J_{ab}^{(2)}$ and $J_{ab}^{(3)}$ values are quite similar in the strong delocalized limit. Yamaguchi et al. claimed that J_{ab} obtained by the approximate spin projection procedure reproduces the characteristic feature of J_{ab} in the whole region, while the other two strategies only work in weak or strong overlap regions.[19b,20a] Although previous studies have showed that spin contamination in DFT is small for the high-spin state,[35] the broken-symmetry singlet state represents a many-particle state with relatively higher spin contamination,[25a,36] which calls for applying a spin projected method.[19b,36b−c] So the $J_{ab}^{(3)}$ values obtained from eq 4 are employed in the following discussions.

The calculated J_{ab} values are sensitive to the choice of computational methods with the LANL2DZ basis set (Table S2). For **2-LT**, the unrestricted symmetry broken calculations in the singlet state[37] computed with USVWN, UBP86, and UBPW91

(26) Wang, J. H.; Becke, A. D.; Smith, V. H., Jr. *J. Chem. Phys.* **1995**, *102*, 3477.
(27) Takano, Y.; Taniguchi, T.; Isobe, H.; Kubo, T.; Morita, Y.; Yamamoto, K.; Nakasuji, K.; Takui, T.; Yamaguchi, K. *Chem. Phys. Lett*. **2002**, *358*, 17.
(28) Ehlers, A. W.; Böhme, M.; Dapprich, S.; Gobbi, A.; Höllwarth, A.; Jonas, V.; Köhler, K. F.; Stegmann, R.; Veldkamp, A.; Frenking, G. *Chem. Phys. Lett.* **1993**, *208*, 111.
(29) Frisch, M. J. et al. *Gaussian 98*, revision A.11.2; Gausian, Inc.: Pittsburgh, PA, 2001.
(30) Glendening, E. D.; Reed, A. E.; Carpenter, J. E.; Weinholk, F. *NBO*, version 3.1.
(31) Frisch, M. J. et al. *Gaussian 03*, revision B.03; Gausian, Inc.: Pittsburgh, PA, 2003.
(32) The energies of singlet and triplet states obtained by the G03 program are lower than those by G98; however all of the J_{ab} values relating to the energy difference, except UB2LYP solutions, are almost the same.
(33) Harris, J. *Phys. Rev. B* **1985**, *31*, 1770.
(34) Schaftenaar, G.; Noordik, J. H. *J. Comput.-Aided Mol. Des.* **2000**, *14*, 123.
(35) (a) Baker, J.; Scheiner, A.; Andzelm, J. *Chem. Phys. Lett*. **1993**, *216*, 380. (b) Pople, J. A.; Gill, P. M. W.; Handy, N. C. *Int. J. Quantum Chem*. **1995**, *56*, 303. (c) Wittbrodt, J. M.; Schlegel, H. B. *J. Chem. Phys.* **1996**, *105*, 6574.
(36) (a) Yamaguchi, K. *Chem. Phys. Lett*. **1975**, *33*, 330. (b) Caballol, R.; Castell, O.; Illas, F.; Moreira, I. de P. R.; Malrieu, J. P. *J. Phys. Chem. A*. **1997**, *101*, 7860. (c) Adamo, C.; Barone, V.; Bencini, A.; Totti, F.; Ciofini, I. *Inorg. Chem*. **1999**, *38*, 1996.
(37) Those BS solutions start from the symmetry broken guess orbitals as referenced by the Gaussian keyword MIX, which are obtained by linear combinations of the symmetry adapted restricted frontier guess orbitals. This option usually produces the open-shell singlet state with spin contamination. Sometimes the BS calculation is automatically converged to the spin restricted solution. In such cases, it should be detected by an application of the STABLE=OPT option to test the stability of the restricted DFT solution. Furthermore, it can be verified by an application of the ALTER option to detect whether a lower energy point may exist.

Table 1. Effective Exchange Integrals (J_{ab})[a] and the Total Spin Angular Momentum Calculated by the UBPW91/LANL2DZ Method for **2-LT**, **2-HT**, and **3-HT** at Their Experimental Structures

dimer	J_{ab}	$\langle S^2\rangle_{BS}$	$\langle S^2\rangle_T$
2-LT	−1466.74	0.0000	2.0045
2-HT	−0.09	0.9828	2.0043
3-HT	28.00	0.9909	2.0043

[a] J_{ab} values from eq 4 are shown in cm^{-1}.

automatically converge to the spin restricted solutions, while BLYP and three hybrid functionals give broken symmetry DFT solutions. The calculated eigenvalues of the stability matrix (Table S3) indicate that the instability of the restricted solution for **2-LT** increases in the order SVWN < BP86 < BPW91 < B3LYP < B3PW91 < BLYP < B2LYP. The order, except BLYP, is parallel to what is expected from the construction of functionals.[38] The larger instability of the DFT solution is usually linked to the larger Hartree−Fock exchange component in the DFT exchange potential.[25a] Therefore, the result of BLYP functional is unusual. Despite the different description of molecular orbital between the closed shell solution and singlet diradical solution,[39] all these results suggest the diamagnetic property for **2-LT**, in qualitative agreement with the experimental observation.[11a] For **2-HT** the J_{ab} values computed with SVWN, BP86, and BPW91 qualitatively agree with the observed weak antiferromagnetic interaction;[11a] however, the opposite trends are obtained with BLYP, B2LYP, B3LYP, and B3PW91. The J_{ab} values for **3-HT** computed with SVWN, BP86, and BPW91 are closer to 10.15 cm^{-1} fitted by the Baker equation,[11b] while larger J_{ab} values are derived with the remaining functionals. Therefore, SVWN, BP86, and BPW91 can provide the reasonable predictions of J_{ab} for $[Ni(mnt)_2]^-$ dimers. In fact, the combination BPW91/LANL2DZ is also recommended by Nyberg et al. for treating metal systems with enough accuracy and reliability.[40] So, we utilized the BPW91/LANL2DZ results to evaluate the magnetic interactions and intermolecular interactions in $[Ni(mnt)_2]^-$ dimers.[41]

As addressed in Figure 2, the calculated J_{ab} values of **2-LT**, **2-HT**, and **3-HT**, as shown in Table 1, can be qualitatively correlated with their energy gaps in the molecular orbital pictures. The absolute value of the energy gap (0.54 eV) of **2-LT** is 9 times that of **2-HT** (0.06 eV), which is consistent with the large difference in J_{ab} values between them. When the gap further decreases to 0.05 eV for **3-HT**, the ferromagnetic contribution competes against the antiferromagnetic contribution and hence the positive J_{ab} value is obtained.

Spin Delocalizations and Polarizations. The distributions of spin density can directly reflect the extent of metal−ligand delocalization. The DFT calculations usually provide reasonable spin densities for the triplet state. In broken symmetry approaches, the spin densities in the singlet state are not strictly related to real spin populations; however they are still useful in describing the magnitude of electron and spin correlations.[18e] Table 2 lists the spin density distributions for **2-LT** and **2-HT** in the singlet state and **3-HT** in the triplet state. At the first glance, the total spin populations on the $[NiS_4]$ are calculated

Table 2. Spin Density Distributions for **2-LT** and **2-HT** in the Singlet State and **3-HT** in the Triplet State[a,b]

dimer	NiS_4	Ni	S	C_1	C_2	N
2-LT	0.000	0.000	0.000	0.000	0.000	0.000
	0.000	0.000	0.000	0.000	0.000	0.000
2-HT	+0.862	+0.203	+0.165	+0.020	−0.005	+0.011
	−0.864	−0.209	−0.164	−0.019	+0.005	−0.011
3-HT	+0.887	+0.215	+0.168	+0.022	−0.006	+0.012
	+0.887	+0.213	+0.169	+0.022	−0.006	+0.012

[a] The second rows in each column are the spin density distributions corresponding to the second layers in the dimer. [b] The structures are shown in Figure 1.

to be about 0.887 in the triplet state, which is close to the experimental results of $\rho_{[NiS4]} = 0.85$.[42] All the spin density distributions of **2-LT** in the singlet state are zero, which are in agreement with the experimental diamagnetic property. However, the spin densities of **2-HT** indicate the weak antiferromagnetic interaction in the singlet ground state. This rationalizes the observed magnetic switching property in complex **2**.[11a] Larger spin density distributions of S atoms (about 0.168 for each S atom, and 0.672 for the ligand S_4) in **3-HT** indicate the strong delocalization effect from the metal Ni atoms to ligands.[42] In addition, the signs of spin densities of the C_1, C_2, and N atoms are alternatively aligned, suggesting the weak spin polarization effects in dimers.

Natural orbitals and their occupation numbers can provide us an insight into understanding the origin of the magnetic interaction for **2-LT**, **2-HT**, and **3-HT** at their experiment geometries. Figure 3 shows SOMOs for **2-LT**, **2-HT**, and **3-HT** in triplet states, respectively. From Figure 3, the singly occupied orbitals of $[Ni(mnt)_2]^-$ monomers in **2-LT** interact with each other, leading to intermolecular bonding and antibonding dimer orbitals. They are greatly delocalized over the dimeric pair with distinct orbital overlaps. The SOMOs for **2-HT** and **3-HT** are almost localized over one $[Ni(mnt)_2]^-$ layer, indicating that the SOMO−SOMO overlap effects are extremely small. The magnetic interaction depends on the competition between the through-space delocalization and exchange integral.[43]

To gain a more quantitative estimation of the extent of spin delocalization and polarization, Table 3 summarizes the occupation numbers of HOMO, SOMOs, and LUMO for **2-LT**, **2-HT**, and **3-HT** in singlet states. The closed-shell structure in **2-LT** is also displayed here by the doubly occupied HOMO ($n_i = 2.0$) and empty LUMO ($n^*_i = 0.0$). From eq 5 the T value of **2-LT** is derived to be 1.00, implying that the strong delocalization exits in **2-LT**. Indeed, the two unpaired electrons coming from two $[Ni(mnt)_2]^-$ units occupy the lowest dimer orbital, leading to the weak interlayer covalent-type bonding, which is partially responsible for the closer S···S separation (3.49 Å, cf. Table S1) compared with the sum of the van der Waals radii (3.70 Å). Such a delocalization picture is clearly shown in the HOMO of **2-LT** (Figure 4). On the basis of occupation numbers of SOMOs, the T_{SOMO} values for **2-HT** and **3-HT** are 0.15 and 0.12, respectively. If we only consider the through-space effect, the antiferromagnetic interaction increases with increasing T_{SOMO}. So the J_{ab} value for **2-HT** (with a larger T_{SOMO} value) should be slightly smaller than that of **3-HT**, as supported by the calculated J_{ab} values. In addition,

(38) Bauernschmitt, R.; Ahlrichs, R. *J. Chem. Phys.* **1996**, *104*, 9047.
(39) Bachler, V.; Olbrich, G.; Neese, F.; Wieghardt, K. *Inorg. Chem.* **2002**, *41*, 4179.
(40) Legge, F. S.; Nyberg, G. L.; Peel, J. B. *J. Phys. Chem. A* **2001**, *105*, 7905.
(41) The effects of large basis sets are not so significant for J_{ab} values as shown in Table S5.
(42) Huyett, J. E.; Choudhury, S. B.; Eichhorn, D. M.; Bryngelson, P. A.; Maroney, M. J.; Hoffman, B. M. *Inorg. Chem.* **1998**, *37*, 1361.
(43) Khan, O.; Briat, B.; Galy, J. *J. Chem. Soc., Dalton Trans.* **1977**, 1453.

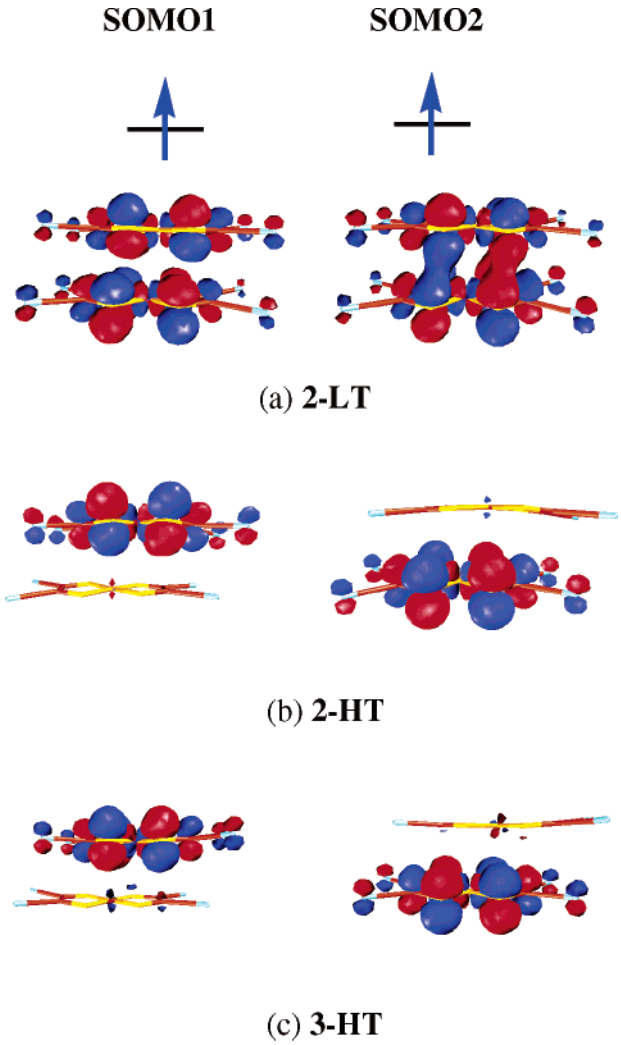

Figure 3. SOMOs of (a) **2-LT**, (b) **2-HT**, and (c) **3-HT** calculated by UBPW91/LANL2DZ in the triplet state, respectively.

Table 3. Occupation Numbers of HOMO, SOMOs, and LUMO as Well as T_{SOMO} for **2-LT**, **2-HT**, and **3-HT** in Singlet States

dimer	HOMO	SOMO1	SOMO2	LUMO	T_{SOMO}
2-LT	2.0000			0.0000	1.00
2-HT	1.9997	1.1463	0.8537	0.0004	0.15
3-HT	1.9997	1.1155	0.8846	0.0004	0.12

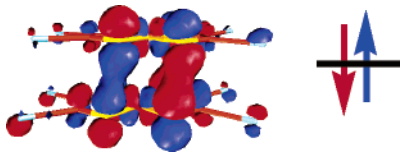

Figure 4. HOMO of the **2-LT** obtained by UBPW91/LANA2DZ in the singlet state with the occupation number of 2.0.

the almost doubly occupied HOMOs (with occupation numbers of 1.9997) and the nearly empty LUMOs (with occupation numbers of 0.0004) indicate that the spin polarization effects are extremely weak in **2-HT** and **3-HT**.

Interlayer Distance Dependence of J_{ab} Values. It is very meaningful to show the effect of interlayer distance, *d*, on the strength of magnetic interactions. Figure 5a illustrates the J_{ab} values by UBPW91 calculations for **2-LT**^{d}, **2-HT**^{d}, and **3-HT**^{d} (the superscript letter ***d*** denotes the change in interlayer distances

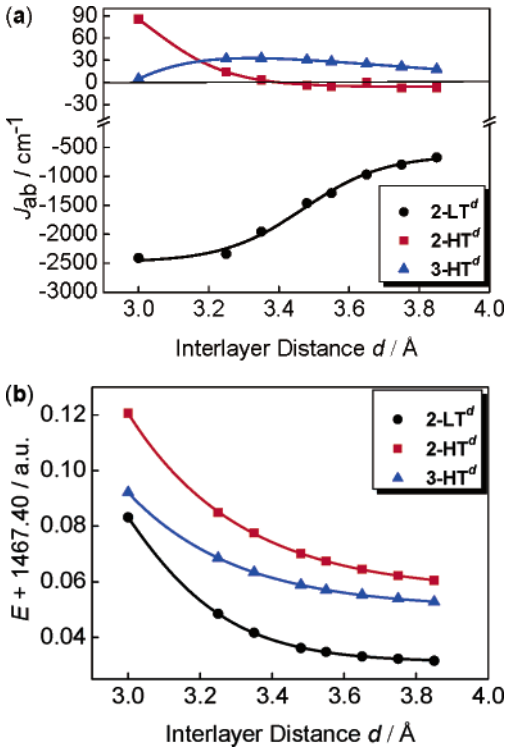

Figure 5. Variations in (a) J_{ab} values and (b) ground-state energies for **2-LT**^{d}, **2-HT**^{d}, and **3-HT**^{d} at their experimental geometries obtained by UBPW91/LANL2DZ with the variation of interlayer distances, *d*. For **2-LT**^{d} and **3-HT**^{d} the ground states are the singlet and triplet states, respectively, while, for **2-HT**^{d}, only the energies of the singlet state are shown.

at their experimental structures). The restricted singlet state for **2-LT**^{d} is kept at the distance of 3.48−3.65 Å. With increasing *d*, the magnitude of antiferromagnetic interaction for **2-LT**^{d} decreases rapidly, and the restricted and unrestricted singlet DFT curves become divergent[44] at the distance of about 3.75 Å ($\langle S^2\rangle_{BS} = 0.0682$). The J_{ab} for **2-HT**^{d} decreases with increasing *d* and becomes negative when the distance is longer than 3.40 Å. Closer inspection of the two curves indicates that no transitions of magnetic interactions[45] occur in **2-LT**^{d} and **2-HT**^{d} during separations from 3.48 to 3.65 Å. The J_{ab} values for **3-HT**^{d} are positive in the whole region and peak at $d = 3.35$ Å, indicating that the transition from the ferromagnetic to diamagnetic does not occur with varying *d*. Obviously, the interlayer distance can affect the strength of magnetic interaction, but changing the interlayer distance *d* solely will not result in an abrupt magnetic switch for **2** and **3**. The extent of slippage (*r* and α) and rotational angle (*θ*) are probably the more important factors to affect the magnetic interactions.

As shown in Figure 5b, the potential curves for **2-LT**^{d}, **2-HT**^{d}, and **3-HT**^{d} are decreasing gradually with increasing intermolecular distance, indicating that the $[Ni(mnt)_2]^-\cdots[Ni(mnt)_2]^-$ interaction is repulsive in the absence of cation. Novoa et al. also addressed this point by studying the $[TCNE]_2^{2-}$ system.[18c] Moreover, we find that the ground-state energies decrease in the order **2-HT** > **3-HT** > **2-LT**, which is in contrast to the increasing order of repulsions **2-HT** < **3-HT** < **2-LT** as expected from the decreasing interlayer distances (**2-HT** (3.65 Å) > **3-HT** (3.55 Å) > **2-LT** (3.48 Å)). So there must be some

(44) This is analogous to the H_2 dissociation problem. For example, see: Goldstein, E.; Beno, B.; Houk, K. N. *J. Am. Chem. Soc.* **1996**, *118*, 6036.
(45) Duclusaud, H.; Borshch, S. A. *J. Am. Chem. Soc.* **2001**, *123*, 2825.

Table 4. Stabilization Energies (kcal/mol) of Bond Interactions between Different Layers Calculated by the UBPW91/LANL2DZ Method for **2-LT** and **2-HT** in the Singlet State and **3-HT** in the Triplet State at Their Experimental Geometries

orbital interactions	**2-LT**	**2-HT**	**3-HT**
	0.32	0.11	0.09
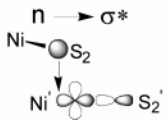	0.12	0.34	0.48

Table 5. Selected NLMO/NPA Bond Orders between Different Layers for **2-LT** in the Singlet State and **2-HT** and **3-HT** in the Triplet State

dimer	Ni–Ni′	∑Ni–S′	∑S–S′
2-LT	0.1459	0.1481	0.3464
2-HT	0.0140	0.0269	0.0037
3-HT	0.0167	0.0288	0.0074

weak bonding interactions contributing to the stability of the isolated $[Ni(mnt)_2]^-$ dimers, **2-LT** and **3-HT**, which will be shown in the next subsection.

Intermolecular Interactions. For a better understanding of the interaction between layers, NBO analysis is carried out at the UBPW91/LANL2DZ level. The NBO results show that three packing patterns **2-LT**, **2-HT**, and **3-HT** have different weak intermolecular interactions. Table 4 displays important bond interactions, $\sigma \rightarrow \sigma^*$ and $n \rightarrow \sigma^*$, and their NBO stabilization energies for all those systems. The interactions between the Ni−S bonding and antibonding orbitals in each monomer, $\sigma \rightarrow \sigma^*$, for **2-LT**[46] (0.32 kcal mol^{-1}) are stronger than those for **2-HT** (0.11 kcal mol^{-1}) and **3-HT** (0.09 kcal mol^{-1}). These strong interactions in **2-LT** can be ascribed to two factors. One is the shorter interlayer distance *d* (3.48 Å), and the other is its nearly eclipsed packing pattern, allowing the maximum overlap of orbitals for **2-LT**. The large slippages (as reflected by Figure 1 and Table S1) in **2-HT** and **3-HT** greatly compress the $\sigma \rightarrow \sigma^*$ interactions but provide a chance to promote the $n \rightarrow \sigma^*$ interactions. As expected, the $n \rightarrow \sigma^*$ interactions in **2-HT** (0.34 kcal mol^{-1}) and **3-HT** (0.48 kcal mol^{-1}) are stronger than that in **2-LT** (0.12 kcal mol^{-1}). The shortest Ni···S′ distance (3.60 Å) in **3-HT** permits the strongest $n \rightarrow \sigma^*$ interaction with the largest stabilization energy among all the studied systems.

The bond interaction results suggest that some weak through-space bondings may exist in dimers. The natural localized molecular orbitals/natural population analysis (NLMO/NPA) bond orders[21] in Table 5 indicate weak intermolecular chemical bonding, especially in **2-LT**. The total bond orders of Ni···Ni′, Ni···S′, and S···S′ for **2-LT** are greatly larger than those for **3-HT** and **2-HT**, implying that the strongest intermolecular stabilization effect exits in **2-LT** to overcome the large repulsion caused by its shortest interlayer distance. This accounts well for the above-mentioned trend in stability of **2-LT** > **3-HT** > **2-HT** (Figure 5b). By closer inspection of **2-LT**, the maximum bond order of S···S′ is calculated to be 0.0748, which corresponds to the intermolecular distance of 3.49 Å (shorter than the van der Waals radii of 3.70 Å). Similar phenomena can be found in other radical materials.[6,47] An unexpected feature found here is the considerably large bond order of Ni···Ni′ (0.1459) corresponding to 3.55 Å, which implies that we should consider the π-Ni van der Waals radius.[18c] Obviously, the cooperative effect of weak intermolecular chemical bondings results in the formation of diamagnetic character for **2-LT**. These intermolecular interactions may be the intrinsic driving force to induce the switchable behavior. Just like 1,3,5-trithia-2,4,6-triazapentalenyl (TTTA) radical,[6a,b] complex **2** was found to undergo a first-order crystallographic phase transition accompanied by lattice dimerization,[11a] which is different from the transfer of two electrons between the t_{2g} and e_g orbitals in the Fe(II) complex.[3−5]

Magnetic Behaviors of Packing Models

It can be concluded from the above discussions that different packing patterns have different effects on magnetic interactions and intermolecular interactions. Further study on the relationship between packing patterns and switchable properties is of great importance. The features of packing patterns can be illustrated by the extent of slippage (*r* and α) and rotational angle θ specified in Figure 1a. We averaged geometrical parameters in model systems **2-LT′**, **2-HT′**, and **3-HT′** to investigate the dependence of J_{ab} values on the geometrical distortions. In the selected model systems **2-LT′**, **2-HT′**, and **3-HT′**, the atomic coordinates of each $[Ni(mnt)_2]^-$ layer are assumed to be planar and perfectly symmetrical (D_{2h}) as shown in Figure 6a; however the packing parameters (*d*, *r*, α, and θ) for each model structures are the same as those in X-ray structures as illustrated in Figure 1. The calculated J_{ab} values of **2-LT′**, **2-HT′**, and **3-HT′** are listed in Table 6. The differences of magnetic interactions between X-ray structures (Table 1) and model structures are

(46) There are several such effective $\sigma \rightarrow \sigma^*$ interactions with comparable stabilization energies in **2-LT** (around 0.19∼0.32 kcal/mol); for the sake of simplicity only the largest stabilization energy of 0.32 kcal/mol is adopted in discussions.

(47) $[Ni(mnt)_2]^-$ can be conceived as an open-shell *radical* anion. For example, see ref 9c.

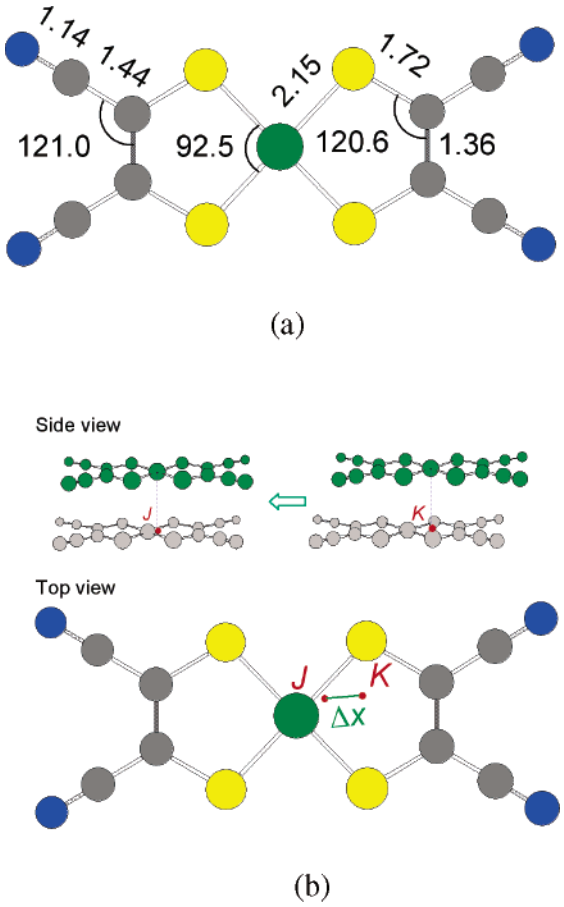

Figure 6. (a) Averaged bond distances (in units of angstrom) and angles (in units of degree) used for the $[Ni(mnt)_2]^-$ model monomer. (b) Side views and top views of the models, and in the latter the upper $[Ni(mnt)_2]^-$ part is omitted for clarity. The sites *J* and *K* represent the extent of slippage (slipping distance *r* and deviation angle α), same as that in **2-LT** and **2-HT**, respectively, while the interlayer distance *d* and rotational angle *θ* are fixed at 3.55 Å and 0°, respectively. The calculations are performed with linear shifting of the extent of slippage from site *K* to *J* with the displacement of Δ*x*. The operations for atoms are colored using the following scheme in side views of the models: light gray, fixed; olive, slipped.

Table 6. Effective Exchange Integrals (J_{ab})[a] and the Total Spin Angular Momentum Calculated by UBPW91/LANL2DZ for **2-LT′**, **2-HT′**, and **3-HT′** at Their Model Structures

model	J_{ab}	$\langle S^2\rangle_{BS}$	$\langle S^2\rangle_T$
2-LT′	−1271.70	0.0000	2.0044
2-HT′	−19.05	0.9717	2.0043
3-HT′	35.69	0.9948	2.0043

[a] J_{ab} values from eq 4 are shown in cm^{-1}.

acceptable, indicating that the slight distortion has little influence on the nature of magnetic coupling. The systematic overestimations of J_{ab} values by using the model structures, **2-LT′** and **3-HT′**, can be contributed to J_{AF} from the configuration interaction of asymmetric molecules in the solid state.[48] Therefore, we can use the averaged planar parameters of $[Ni(mnt)_2]^-$ instead of the distorted geometries to explore the stacking effect.

We vary the extents of slippage and rotational angles based on the averaged parameters to explore the relationship between packing patterns and the magnetic switching property. The

(48) Shultz, D. A.; Fico, R. M., Jr.; Bodnar, S. H.; Kumar, R. K.; Vostrikova, K. E.; Kampf, J. W.; Boyle, P. D. *J. Am. Chem. Soc.* **2003**, *125*, 11761.

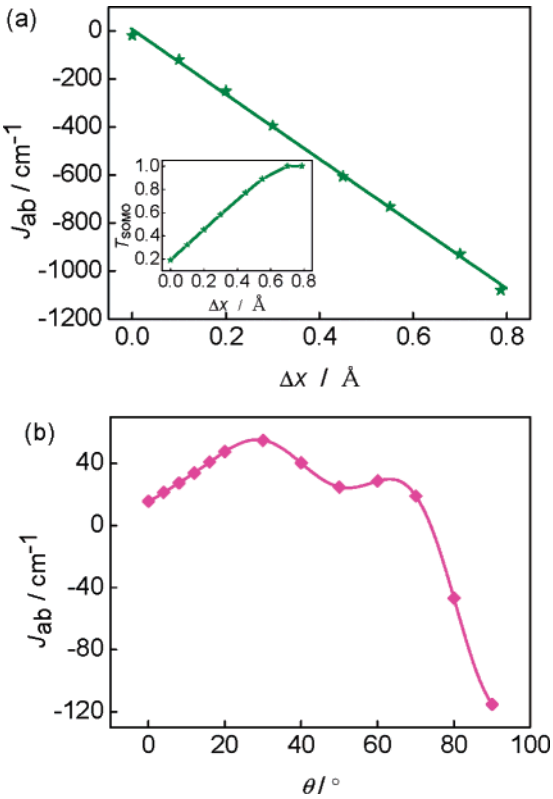

Figure 7. J_{ab} values varied with (a) linear shifting of the extent of slippage from site *K* to *J* (Δ*x*) (inset: T_{SOMO} versus Δ*x*) and (b) different rotational angles *θ*.

interlayer distance *d* is fixed at 3.55 Å. As shown in Figure 6b, the relative positions of projection site of the central metal atom, *J* and *K*, represent the extent of slippage (slipping distance *r* and deviation angle α), which are the same as those in **2-LT** and **2-HT**, respectively. Considering only the effect of slippage, we fix the rotational angle at 0° and perform UBPW91/LANL2DZ calculations with a linear shifting from site *K* to *J* with the displacement of Δ*x*. Furthermore, we vary only the rotational angle for **3-HT′** to explore whether this factor contributes to the switching property in complex **3**.

Figure 7a and b show the variations of J_{ab} values, varying with Δ*x* and *θ*, respectively. The J_{ab} values decrease rapidly and linearly with changing the extent of slippage as shown in Figure 7a. The $[Ni(mnt)_2]^-$ dimer almost forms the closed-shell pair at $\Delta x = 0.70$ Å, as estimated from the T_{SOMO} vs Δ*x* curve (inset of Figure 7a). Obviously, the magnetic character can change from the weak antiferromagnetic interaction to the diamagnetic form upon varying the extent of slippage. However, the switch property promised by the abrupt change from site *K* to *J* is achieved by the first-order phase transition in the experiment.[11a] Therefore, the abrupt modulation of the extent of slippage is probably the dominating factor for the switching property of complex **2**. As shown in Figure 7b, there are two peaks in the J_{ab} curves at $\theta = 30°$ and 60°. Interestingly, the adjustment of the packing patterns by rotating angle *θ* changes the sign of J_{ab}, corresponding to a transition of magnetic interactions between 54.85 and −115.22 cm^{-1}, but it is still insufficient to approach the diamagnetic regime.[45] Therefore, we exclude the factor of rotational angle and assume that only the extent of slippage should be the crucial factor to affect the abrupt magnetic transition for complex **3**.

As mentioned above, the abrupt change of the extent of slippage provides new possibilities for the design of molecular magnetic switching devices.[6,8] For most of the potential applications, the transition must occur around room temperature.[4,6,7c] Therefore, we prefer to choose a stacking pattern corresponding to a diamagnetic form slightly below room temperature. If the condition of the first-order phase transition around ambient temperature is also satisfied, the room-temperature magnetic switching will be obtained. For such a purpose, we should increase the magnitude of intermolecular interactions such as hydrogen bonding and $\pi-\pi$ stacking in the complex. If the degree of cooperative effects is moderate, a room-temperature magnetic bistability with a wide thermal hysteresis loop may occur.[4−8] We are experimentally pursuing this line of research.

Concluding Remarks

We have performed UBPW91 calculations as well as NO and NBO analyses for various $[Ni(mnt)_2]^-$ dimers with different stacking patterns to elucidate the magnetic interactions and the physical pictures of the weak intermolecular bonding interactions. The stacking patterns have been demonstrated to be an important factor in magnetic interactions of $[Ni(mnt)_2]^-$ dimers. The calculated results of complex **2** are in agreement with the previous experimental phenomena that the material exhibits a transition from paramagnetic to diamagnetic as temperature is lowered. In addition, the J_{ab} value of 28.00 cm^{-1} for **3-HT** by BPW91/LANL2DZ calculation is also consistent qualitatively with the observed ferromagnetic interaction. The spin-delocalization picture has been presented by NO analysis, from which we find that the delocalization is favored by eclipsed stacking and shorter interlayer distance. The weak intermolecular chemical bondings have been demonstrated by the NBO analysis, which accounts well for the difference in the thermodynamic stabilities of dimers. The cooperative effect of this kind of weak intermolecular bondings (Ni···Ni′, Ni···S′, and S···S′) is responsible for the diamagnetic character below the transition temperature and may be the intrinsic driving force to induce the first-order crystallographic phase transition accompanied by lattice dimerization. Furthermore, our systematic investigations at different interlayer distances d, extents of slippage (slipping distance r and deviation angle α), and rotation angles θ provide more illustrations to show magnetostructural correlations. The abrupt modulation of the extent of slippage by external perturbations creates new possibilities for the design of molecular magnetic switching devices.

Acknowledgment. This project was financially supported by the National Natural Science Foundation of China (Grant Nos. 20490218, 90303020, and 20433020).

Supporting Information Available: Summary of intra- and intermolecular distances for **2-LT**, **2-HT**, and **3-HT** at their experimental geometries (Table S1); total energies and total spin angular momentum for the singlet and triplet states, and the J_{ab} values using three computational schemes for **2-LT**, **2-HT**, and **3-HT**, obtained by USVWN, UBP86, UBPW91, UBLYP, UB2LYP, UB3LYP, and UB3PW91 calculations with the LANL2DZ basis set at their experimental geometries with the Gaussian 98 program (Table S2); the eigenvalue of the stability matrix and energy lowerings ΔE for **2-LT** calculated at various levels of DFT in the singlet state (Table S3); total energies and the J_{ab} values for **2-LT**, **2-HT**, and **3-HT** obtained by several DFT functional calculations with the LANL2DZ basis set at their experimental geometries with the Gaussian 03 program (Table S4); total energies and the J_{ab} values for **2-LT**, **2-HT**, and **3-HT** obtained by UBPW91 functional calculations with several basis sets at their experimental geometries with the Gaussian 98 program (Table S5); total energies and the J_{ab} values for **2-LT**^{d}, **2-HT**^{d}, and **3-HT**^{d} calculated by UBPW91/LANL2DZ, with different interlayer distances d on the basis of their experimental geometries (Table S6); total energies and the J_{ab} values for **2-LT′**, **2-HT′**, and **3-HT′** calculated by UBPW91/LANL2DZ at their model structures (Table S7); total energies, J_{ab} values, and T_{SOMO} calculated by UBPW91/LANL2DZ with linear shifting of the extent of slippage from site K to J, Δx, on the basis of the model structures (Table S8); total energies and the J_{ab} values calculated by UBPW91/LANL2DZ with different rotation angles θ on the basis of model structures (Table S9); complete refs 2g, 9f, 10a, c, d, 29, and 31. This material is available free of charge via the Internet at http://pubs.acs.org.

JA050631Z